

A Journal of the German Chemical Society

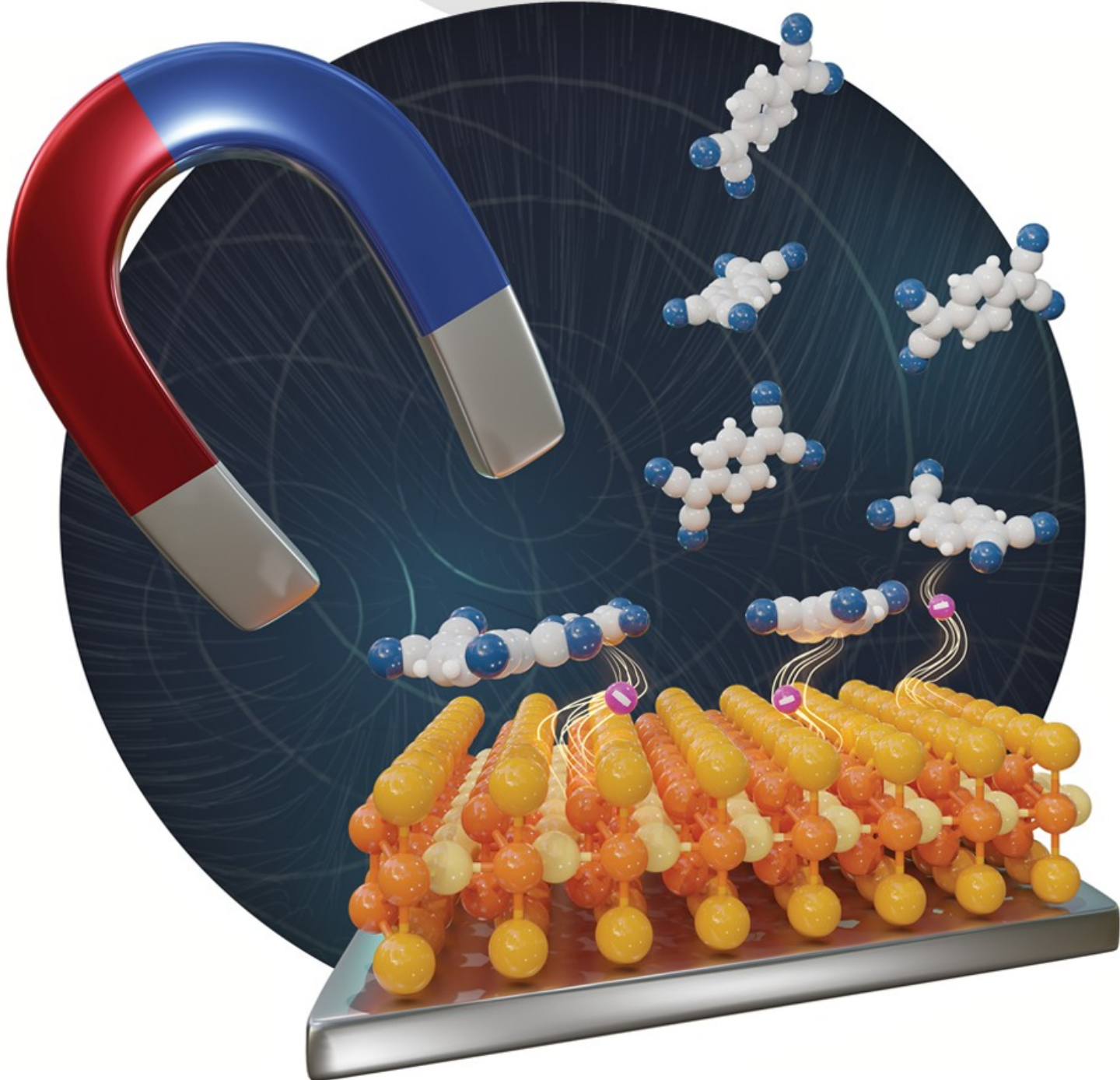
Angewandte

Chemie

International Edition

GDCh

www.angewandte.org



Deposition of organic acceptor molecules, 7,7,8,8-tetracyanoquinodimethane (TCNQ), on the surface of ferromagnetic Fe_3GeTe_2 (FGT) nanosheets causes an unprecedented 5-fold increase in the coercivity of the FGT-TCNQ composite as compared to that of the bare nanosheets. This huge coercivity enhancement has been traced to the electron transfer from FGT to TCNQ that strengthens the interlayer magnetic exchange in FGT, as illustrated by José J. Baldoví, Michael Shatruk et al. in their Research Article (e202412425).

WILEY  VCH



Opening the Hysteresis Loop in Ferromagnetic Fe_3GeTe_2 Nanosheets Through Functionalization with TCNQ Molecules

Govind Sasi Kumar, Alberto M. Ruiz, Jaime Garcia-Oliver, Yan Xin, José J. Baldoví,* and Michael Shatruk*

Abstract: Ferromagnetic metal Fe_3GeTe_2 (FGT), whose structure exhibits weak van-der-Waals interactions between 5-atom thick layers, was subjected to liquid-phase exfoliation (LPE) in N-methyl pyrrolidone (NMP) to yield a suspension of nanosheets that were separated into several fractions by successive centrifugation at different speeds. Electron microscopy confirmed successful exfoliation of bulk FGT to nanosheets as thin as 6 nm. The ferromagnetic ordering temperature for the nanosheets gradually decreased with the increase in the centrifugation speed used to isolate the 2D material. These nanosheets were resuspended in NMP and treated with an organic acceptor, 7,7,8,8-tetracyanoquinodimethane (TCNQ), which led to precipitation of FGT-TCNQ composite. The formation of the composite material is accompanied by charge transfer from the FGT nanosheets to TCNQ molecules, generating $\text{TCNQ}^{\bullet-}$ radical anions, as revealed by experimental vibrational spectra and supported by first principles calculations. Remarkably, a substantial increase in magnetic anisotropy was observed, as manifested by the increase in the coercive field from nearly zero in bulk FGT to 1.0 kOe in the exfoliated nanosheets and then to 5.4 kOe in the FGT-TCNQ composite. The dramatic increase in coercivity of the composite suggests that functionalization with redox-active molecules provides an appealing pathway to enhancing magnetic properties of 2D materials.

Introduction

The rapid development of research in 2D materials, spurred by the seminal experimental discovery of graphene,^[1] has opened abundant research opportunities in many areas of chemistry,^[3] physics,^[6] materials science,^[9] engineering,^[13] and biomedicine.^[15] The principal driver of these opportunities is the extremely high sensitivity of the physical properties of one- or few-atom thick 2D materials to both the action of external parameters (strain, light, temperature, electric/magnetic fields) and changes in chemical composition. The chemical modifications can involve not only changes in the composition of the 2D material itself but also introduction of extraneous species, e.g., via surface functionalization of the 2D material with atoms and molecules.

The high surface-to-volume ratio inherent in the ultra-thin 2D materials means that even a relatively small surface coverage with molecular species can have a drastic impact

on material's properties. Both non-covalent modification via physisorption and covalent modification via formation of chemical bonds have been shown to impact, to a different extent, the properties of many common 2D materials, such as graphene, phosphorene, boron nitride, and transition metal dichalcogenides.^[17] Covalent functionalization usually exerts a more pronounced effect on the substrate because the formation of strong molecule-substrate bonds unavoidably causes redistribution of bonding and modification of the electronic structure of the 2D material. In turn, non-covalent functionalization can be considered as a milder and more controllable approach that allows to tune the molecule-substrate interactions by an appropriate choice of the molecules to be absorbed.

Arguably, the molecular species that can actively interact with the underlying substrate through charge transfer can be considered especially attractive for non-covalent functionalization of 2D materials, because the extent of charge transfer can be tuned by adjusting the energies of the frontier molecular orbitals relative to the Fermi level and the band gap of the 2D material. In this vein, organic donor and acceptor molecules have been used to induce, respectively, *n*- and *p*-type doping of 2D semiconductors. For example, several organic acceptors, such as 2,3-dichloro-5,6-dicyano-1,4-benzoquinone (DDQ), 7,7,8,8-tetracyanoquinodimethane (TCNQ), 2,3,5,6-tetrafluoro-7,7,8,8-tetracyanoquinodimethane (F_4TCNQ), tetracyanoethylene (TCNE), and tetrathiafulvalene (TTF), were deposited via electron-beam evaporation on 2D WSe_2 .^[24] These heterostructures functioned as nonvolatile memory devices due to interfacial charge trapping between 2D WSe_2 and the corresponding molecule, and the performance of the devices was found to

[*] G. Sasi Kumar, J. Garcia-Oliver, Prof. Dr. M. Shatruk
Department of Chemistry and Biochemistry
Florida State University
95 Chieftan Way, Tallahassee, FL 32306, United States
E-mail: shatruk@chem.fsu.edu
A. M. Ruiz, Dr. J. J. Baldoví
Instituto de Ciencia Molecular (ICMol)
Universitat de València
Catedrático José Beltrán 2, Paterna, 46980 Spain
E-mail: j.jaime.baldovi@uv.es
Dr. Y. Xin, Prof. Dr. M. Shatruk
National High Magnetic Field Laboratory,
1800 E Paul Dirac Dr,
Tallahassee, FL 32310, United States

correlate with the redox properties of the molecules. Likewise, evaporation of F_4TCNQ onto the surface of 2D MoS_2 led to electron transfer from the 2D substrate to the molecule.^[25] This heterostructure was proposed as NH_3 sensor, as the charge transfer was suppressed in the presence of ammonia molecules. Recent theoretical work also predicted a remarkable increase in the conductivity of 2D InSe upon deposition of TTF^[26] and tunable magnetic anisotropy of 2D CrI_3 upon deposition of either TTF or TCNQ.^[27]

2D magnets represent a special group of ultrathin structures derived from bulk magnetic materials.^[8,28] The reduction in the dimensionality has been shown to have a strong impact on the magnetic properties of such materials as CrI_3 ,^[29] CrSBr ,^[30] and Fe_3GeTe_2 .^[32] Nevertheless, in contrast to 2D semiconductors, functionalization of 2D magnets with molecules has been largely unexplored, although some intriguing results have been reported for thin-film materials. For example, deposition of C_{60} molecules on a thin film of paramagnetic Cu metal led to observation of ferromagnetic ordering, due to electron transfer from Cu to the C_{60} layer.^[34] The aforementioned theoretical work on CrI_3 predicted that the electron or hole doping, depending on the electron transfer from the TTF donor or to the TCNQ acceptor molecules, should lead, respectively, to the decrease or increase in the magnetic anisotropy of the 2D material. Thus, the electron transfer between the physisorbed molecules and the magnetic substrate offers an appealing pathway to modify the magnetic behavior. Metallic (itinerant) magnets are known to exhibit strong coupling between their magnetic properties and electronic band structure,^[35] which makes this type of magnets especially susceptible to effects of chemical doping.^[39]

One of the challenges in studying such heterostructures is the bottleneck created due to the insufficient sensitivity of direct magnetic measurements to detect magnetic properties of the ultrathin flakes of 2D materials. An appealing approach to combat this problem is to prepare such heterostructures on a larger scale, by utilizing the liquid-phase exfoliation (LPE) approach that allows preparation of bulk amounts of 2D materials.^[45] Due to the presence of solvent during the formation of heterostructures, the LPE approach is not as immaculate as mechanical exfoliation and assembly, but it provides an alternative pathway to evaluating the effects of heterostructure formation on the magnetic properties of the underlying 2D substrates. Herein, we report the effect of non-covalent functionalization of the itinerant 2D magnet Fe_3GeTe_2 (FGT) with the well-known organic acceptor, TCNQ. We demonstrate that LPE-generated FGT nanosheets undergo electron transfer to the physisorbed TCNQ molecules, which, in turn, cause a dramatic increase in the apparent magnetic anisotropy of FGT, manifested as the increase in the coercivity from nearly 0 in the bulk material to 5.4 kOe in the FGT-TCNQ composites.

Results and Discussion

Synthesis and Liquid-Phase Exfoliation

Crystalline Fe_3GeTe_2 (FGT) was synthesized by chemical vapor transport following the previous report.^[48] The crystals were shiny metallic plates with optically smooth (001) faces that measured up to few mm^2 in the surface area. The unit cell parameters determined by single-crystal X-ray diffraction ($a=4.002(3)$ Å and $c=16.36(2)$ Å in the $P6_3/mmc$ space group) matched well those reported in the literature ($a=4.0045$ Å and $c=16.376$ Å).^[48] The phase purity of the sample was confirmed by powder X-ray diffraction (PXRD), which also revealed strong preferred orientation along the [001] direction (Figure 1). The unit cell refinement from the PXRD data yielded the lattice parameters $a=4.000(8)$ Å and $c=16.42(4)$ Å, which agreed well with those determined by single-crystal X-ray diffraction.

The crystal structure of FGT is composed of 5-atom thick slabs, in which the atomic layers alternate in the Te–Fe–(Ge,Fe)–Fe–Te sequence (Figure 2). These slabs, terminated by Te atoms, exhibit weak interlayer van-der-Waals interactions, with nearest Te···Te distance of 3.74 Å. Therefore, the material can be easily exfoliated both by the mechanical (“scotch-tape”) method and by the LPE method used in this work.

The LPE was performed according to the general established protocol,^[47] which involves ultrasonication of a powder sample in appropriate solvent followed by a series of size-selective centrifugations to isolate sheets of different thicknesses (Figure S1). Prior to the sonication, the phase-pure FGT powder was soaked in N-methyl pyrrolidone (NMP) for 2 h, to improve the efficiency of exfoliation. NMP was chosen as the LPE solvent based on multiple reports of its surface tension matching very well the surface energies of various van-der-Waals materials.^[49] The LPE attempts were also performed in other solvents, but they

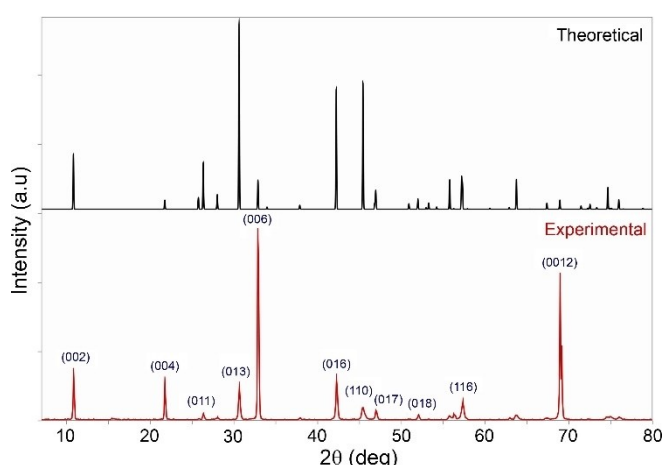


Figure 1. The theoretical and experimental PXRD patterns of Fe_3GeTe_2 , with the corresponding (hkl) lattice planes indicated for the experimental peaks. The theoretical pattern was simulated with the 0.1° peak width.

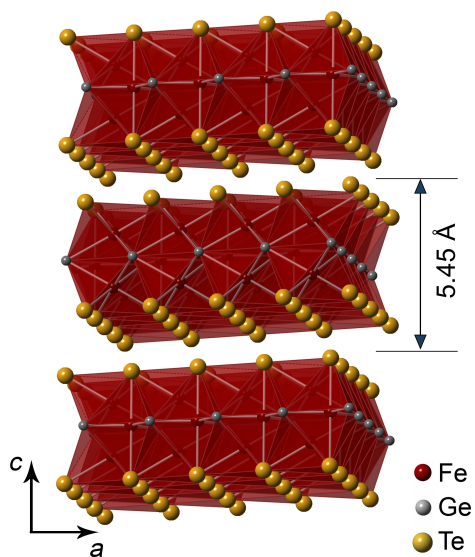


Figure 2. Crystal structure of Fe_3GeTe_2 , viewed nearly perpendicular to the c axis and presented as layers of Fe-centered polyhedra built of Ge and Te atoms.

were not as successful as those using NMP, as judged by rapid precipitation of the exfoliated sheets. Also, it was crucial to carry out the LPE under inert atmosphere since the mechanically exfoliated FGT sheets were shown to be prone to surface oxidation.^[52]

The pre-soaked sample was ultrasonicated in NMP for a longer time (6–7 h). The absence of signs of precipitation after ultrasonication revealed the stability of exfoliated sheets in NMP. The ultrasonication was followed immediately by centrifugation at 1000 rpm for 30 min to remove the large fraction of non-exfoliated particles. The remaining supernatant was subjected to a series of centrifugations with speeds ranging from 2000 rpm to 9500 rpm. The precipitate collected at each step was re-dispersed in a small amount of NMP (2–3 mL) and labelled with the corresponding centrifugation speed. The re-dispersed suspensions remained stable under inert conditions for almost 8 weeks. The PXRD pattern collected on the sample isolated at 2000 rpm (Figure S2) confirmed that the structural integrity was preserved after ultrasonication and centrifugation. The exfoliated samples tend to lose the preferred orientation, which was prevalent in the bulk samples, and exhibit slight broadening of the PXRD peaks which is attributed both to the reduction in the thickness of the material and to introduction of some strain due to ultrasonication. The Raman spectrum of the exfoliated sheets also matched the Raman spectrum of the bulk material, with the main vibrational modes observed at $\sim 120 \text{ cm}^{-1}$ and $\sim 140 \text{ cm}^{-1}$ (Figure S3).

Since NMP is a high-boiling solvent, the exfoliated sheets were precipitated by adding a water-ethanol mixture (1:1 v/v) and re-dispersed in isopropyl alcohol (IPA) for microscopic imaging. The fresh suspension of sheets in IPA was drop-cast onto SiO_2/Si wafers and analyzed using scanning electron microscopy (SEM). The SEM images (Figure 3a and S4) clearly show successful exfoliation of the

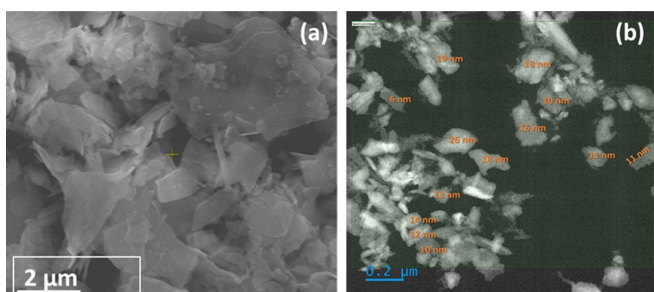


Figure 3. SEM (a) and annular-dark-field STEM (b) images of exfoliated Fe_3GeTe_2 isolated at 2000 rpm. See the Supporting Information for additional electron micrographs.

bulk FGT into nanosheets. The observed clustering of sheets can be explained by the instability of the suspension in IPA.

To estimate the thickness of the exfoliated sheets, dilute IPA suspensions were drop-cast on formvar/carbon coated 200-mesh Cu grids and examined by scanning transmission electron microscopy (STEM) with electron-energy loss spectroscopy (EELS). The log-ratio EELS analysis of the sheets collected at 2000 rpm (Figure 3b and S5) revealed that the thickness of the sheets varied from 6 nm to 19 nm, which corresponds to ~ 11 to ~ 35 five-atom-thick slabs, given that the slab thickness in the structure of FGT is $\sim 0.545 \text{ nm}$ (Figure 2).

Preparation of Fe_3GeTe_2 -TCNQ Heterostructures

Given previous reports of facile reactivity of TCNQ with metallic surfaces,^[53] we hypothesized that this organic acceptor should have a good affinity to the metallic FGT ferromagnet. To prepare the heterostructures, the exfoliated sheets collected at 2000 rpm were re-dispersed in NMP and mixed with a solution of TCNQ in NMP, in an approximate FGT/TCNQ molar ratio of 1:1. Although the suspension of FGT sheets remained stable on its own for weeks, the addition of TCNQ caused precipitation of the suspension after ~ 3 h, clearly supporting the expected interaction between the FGT surface and TCNQ molecules. Nevertheless, the precipitation was slow, and the precipitate was collected after 5 days, to ensure the completeness of the reaction. After this time, the supernatant solution became pale-green, suggesting that most of TCNQ had been precipitated with the FGT sheets (Figure 4).

The PXRD analysis of the FGT-TCNQ composite revealed that its diffraction pattern is very similar to that of the bare FGT nanosheets isolated at 2000 rpm (Figure S6). Therefore, the composite is likely to contain TCNQ molecules absorbed on the FGT sheets and dispersed between them, as the experimental PXRD patterns reveal the lack of any substantial amount of neutral TCNQ that could have been co-crystallized with the FGT-TCNQ composite.

The green coloration of the supernatant left after the co-precipitation of FGT and TCNQ was a strong indicator that TCNQ molecules had been reduced to TCNQ^- anions. To

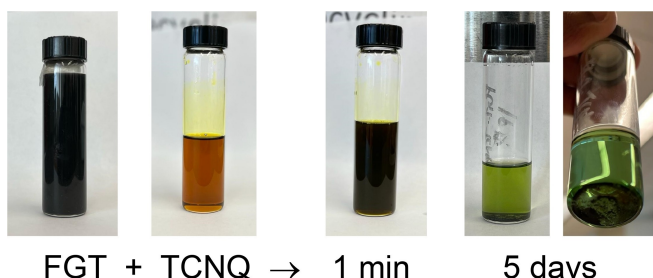


Figure 4. Photographs of the suspension of FGT sheets in NMP and a solution of TCNQ in NMP taken prior to mixing and then 1 min and 5 days after the two reactants had been mixed.

estimate the charge (δ) of TCNQ in the heterostructure, we used infrared (IR) spectroscopy to monitor the characteristic stretching frequency (ν_{CN}) of the TCNQ nitrile groups, taking advantage of the relationship $\nu_{\text{CN}} = 44\delta + 2227$.^[55] The ν_{CN} stretch was observed to shift from 2227 cm^{-1} in neutral TCNQ to 2190 cm^{-1} in the FGT-TCNQ heterostructure (Figure 5a), which corresponds to the average charge of -0.84 per TCNQ molecule. The reduction of TCNQ molecules can be attributed to electron transfer from the metallic FGT sheets due to the electron-accepting nature of TCNQ. The loss of the absorption band at 2227 cm^{-1} in the IR spectrum of the FGT-TCNQ composite indicates the complete reduction of TCNQ molecules to $\text{TCNQ}^{\bullet-}$ anion-radicals.

Interestingly, the IR spectrum of the FGT-TCNQ composites collected after only 4 h from the time of mixing showed ν_{CN} stretches at both 2175 cm^{-1} and 2225 cm^{-1} (Figure S7), thus indicating that the reduction of TCNQ was incomplete. It is possible that some neutral TCNQ molecules were trapped by the precipitating composite. Therefore, it is important to let the precipitation proceed for several days to achieve the complete reaction.

Supporting evidence for the charge transfer was obtained by examining Raman spectra, which also are highly sensitive to the charge on TCNQ. Due to the resonance Raman effect, strong symmetric bands were observed in the spectrum. Generally, a large shift in the $\text{C}=\text{C}$ bond

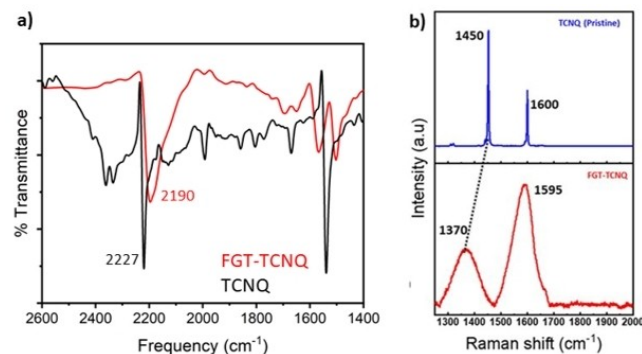


Figure 5. Infrared (a) and Raman (b) spectra of neutral TCNQ in comparison to the FGT-TCNQ heterostructures.

stretching frequency is observed as the charge on the TCNQ molecule varies. For example, the stretching frequencies of $\sim 1438\text{ cm}^{-1}$ and $\sim 1390\text{ cm}^{-1}$ were reported for the neutral and anionic TCNQ, respectively, although small variations of these values were observed due to crystal field effects.^[56] The Raman spectra recorded in the present work revealed a shift in the $\text{C}=\text{C}$ stretching frequency from 1450 cm^{-1} in neutral TCNQ to 1370 cm^{-1} in the FGT-TCNQ heterostructure (Figure 5b), in agreement with the values reported in the literature for the TCNQ molecule and $\text{TCNQ}^{\bullet-}$ anion-radical, respectively.^[56] We should note, however, that both IR and Raman absorption bands observed for the FGT-TCNQ heterostructure were much broader than those recorded for pristine TCNQ, which suggests some variability in the charge distribution over the anionic TCNQ species in the heterostructure.

Magnetic Properties

Temperature dependence of magnetic susceptibility (Figure 6a) measured on the bulk polycrystalline sample of FGT revealed the ferromagnetic ordering of Fe moments below a Curie temperature (T_C) of 221 K .^[57] The ordering temperature is slightly lower than the expected $T_C=230\text{ K}$ reported earlier,^[58] which could be attributed to the small Fe deficiency in the crystal structure.^[59] The field-dependent magnetization measurements (Figure 6b) confirmed that bulk FGT is a soft ferromagnet with coercivity (H_c) near zero. The maximum magnetization observed at 7 T was $1.5\text{ }\mu_{\text{B}}$ per Fe atom ($4.5\text{ }\mu_{\text{B}}$ per formula unit), also in good

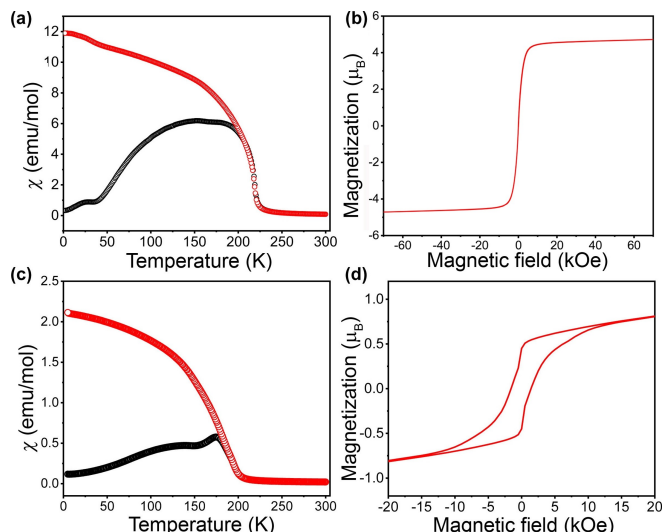


Figure 6. (a) The temperature dependence of magnetic susceptibility of the bulk FGT crystals measured in the ZFC (black) and FC (red) regimes. (b) A magnetic hysteresis plot for the FGT crystals measured at 1.8 K . (c) The temperature dependence of magnetic susceptibility of the FGT sheets isolated at 2000 rpm , measured in the ZFC (black) and FC (red) regimes. (b) A magnetic hysteresis plot for the exfoliated FGT sheets measured at 1.8 K .

agreement with the previously reported value of $1.6 \mu_B$ per Fe atom.

An advantage of the LPE technique (relative to mechanical exfoliation) is that it provides enough exfoliated material to perform conventional magnetic measurements typically used for bulk samples. Initial measurements on the exfoliated sheets were carried out on samples re-dispersed in NMP to assess magnetic behavior of isolated sheets. The weak diamagnetism of NMP did not impact the measurements significantly. Temperature dependence of the magnetic susceptibility of the sheets collected at 2000 rpm (Figure 6c) clearly showed the decrease in T_C to 213 K. Moreover, a pronounced effect of thickness reduction on the magnetic properties was manifest in the opening of the hysteresis to the coercivity value $H_c = 1.01$ kOe (Figure 6d). This increase in the coercivity indicates a substantial increase in the magnetic anisotropy of the exfoliated sheets as compared to the bulk FGT. This observation is also in agreement with the reported opening of the hysteresis loop for FGT nanoflakes prepared by mechanical exfoliation.^[60]

Similar to the sheets isolated at 2000 rpm, magnetic measurements on the sheets isolated between 3000 to 8000 rpm showed the decrease in T_C (Figure S8a). The value of T_C became progressively smaller as the centrifugation speed (ω) increased, in agreement with the decrease in the lateral size and thickness of the sheets collected at higher speeds. The lowest T_C value of 185 K, observed for the sheets isolated at 8000 rpm, was similar to that reported for mechanically exfoliated bilayers of FGT.^[33] Interestingly, we observed a linear dependence between T_C and ω (Figure S8b).

The observation of enhancement in the coercivity for the initially exfoliated FGT nanosheets vs. the bulk material suggests that the magnetic behavior of the sheets is highly sensitive to the nature of their surfaces. Therefore, the magnetic properties were studied for the composite obtained by reacting FGT sheets isolated at 2000 rpm with a solution of TCNQ in NMP. The FGT-TCNQ heterostructure showed $T_C = 198$ K (Figure 7a), similar to $T_C = 213$ K observed for the sheets alone. The slight decrease in the T_C value might be associated with the effective hole doping of the FGT nanosheets due to electron transfer to the TCNQ molecules in the heterostructure. Indeed, such an effect of hole doping

was reported for mechanically exfoliated FGT nanoflakes.^[61] Although the same work reported rapidly decreasing coercivity with hole doping, we observed a dramatic increase in coercivity in the FGT-TCNQ heterostructures. The field-dependent magnetization measured at 1.8 K revealed widening of the hysteresis loop to $H_c \approx 5.4$ kOe, which is five times higher than that recorded for the bare nanosheets (Figure 7b). Therefore, the formation of the composite and the FGT to TCNQ charge transfer led to a drastic increase in the apparent magnetic anisotropy of the resulting material. We would like to point out that, in the present case, the hole doping is achieved by FGT-to-TCNQ electron transfer, while in the mentioned earlier work it was a result of creation of iron vacancies in the bulk FGT that was later subjected to mechanical exfoliation. To further understand the charge transfer in the composite FGT-TCNQ material and to gain insight into the effects of hole doping, we turned to first-principles calculations.

Theoretical Study

We began our theoretical analysis by calculating structural and electronic properties of a single 5-atom thick layer of FGT using density functional theory (DFT). We used the local density approximation (LDA) as exchange-correlation functional, as it has been shown to provide an adequate description of the properties of FGT.^[62] We did not include the Hubbard-U correction, frequently used for systems with *d*-orbitals, because it was shown to overestimate both the lattice parameters and magnetic moments of bulk FGT relative to the experimental values.^[59,65] Our DFT calculations predicted the basal lattice parameter $a = 3.92$ Å, in good agreement with previous reports and with the experimental value of $4.002(3)$ Å. Spin-polarized calculations led to the magnetic moments of $1.92 \mu_B$ for the Fe(1) sites, located closer to the outer Te atoms, and $1.09 \mu_B$ for the Fe(2) sites, located in the middle of the layer (Figure S9). Given the 2:1 ratio of these atoms, the average moment of $1.40 \mu_B$ per Fe atom is in excellent agreement with the experimental value of $1.45 \mu_B$. The spin-polarized band structure (Figure S9) agrees with the metallic nature of this material.

To investigate the interaction between TCNQ and FGT, a single molecule of TCNQ was positioned over a 4×4 supercell of the single FGT layer. Such a model results in the distance of at least 7 Å to the next TCNQ molecule, ensuring no significant electrostatic interaction between the absorbed molecules. Six different configurations for the deposition of TCNQ on FGT were optimized (Figure 8). The electrostatic interactions between FGT and TCNQ were analyzed by evaluating the adsorption energy, defined as $E_{ads} = E_{FGT-TCNQ} - (E_{FGT} + E_{TCNQ})$, where $E_{FGT-TCNQ}$, E_{FGT} , and E_{TCNQ} are total energies of the hybrid FGT-TCNQ heterostructure, pristine FGT, and TCNQ, respectively. The value of E_{ads} is exothermic in all six cases (Table 1), indicating thermodynamic stability of all proposed configurations. The most stable adsorption is found for the four N termini of the TCNQ molecule residing on top of four Ge

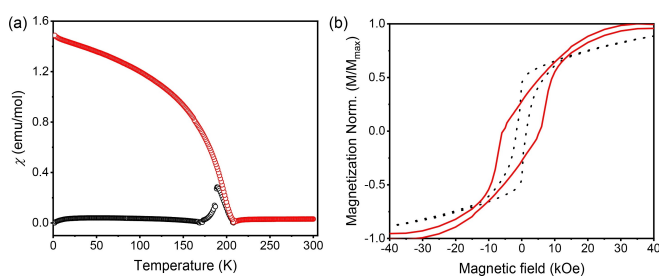


Figure 7. Magnetic properties of the FGT-TCNQ heterostructure: (a) The temperature dependence of ZFC (black) and FC (red) magnetic susceptibility measured under applied field of 100 Oe. (b) Normalized magnetic hysteresis plot (red) measured at 1.8 K and its comparison to the hysteresis of the bare exfoliated sheets (black).

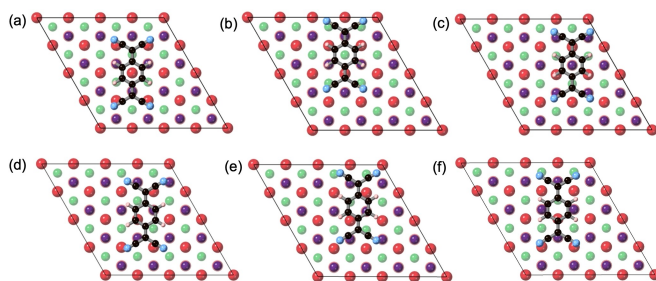


Figure 8. Top views of a TCNQ molecule adsorbed at different sites of the single FGT layer, with the center of the molecule located above the Fe (a), Ge (b), or Te (c) atoms or above the Fe–Te (d), Ge–Te (e), or Fe–Ge (f) bonds. Color code: Fe = red, Ge = green, Te = dark blue, C = black, N = light blue, H = pink.

sites (Figure 8b), with $E_{\text{ads}} = -3.14 \text{ eV}$. The favorable nature of these interactions is also confirmed by the side view of the six FGT-TCNQ models (Figure S10), which reveals a bending distortion of the TCNQ molecule, aiming to optimize the interactions between the N termini and the substrate.

It is worth mentioning that TCNQ was already theoretically predicted to be stable over such substrates as CrI_3 or arsenene, with E_{ads} values of -0.70 and -1.38 eV , respectively.^[27,66] Much stronger substrate-molecule interactions, however, are predicted by our calculations on the FGT-TCNQ heterostructures. We attribute this difference to the much lower work function expected for FGT, in comparison to CrI_3 or arsenene, which should lead to a facile electron transfer from the metallic layer to the adsorbed TCNQ molecules. To evaluate the extend of the electron transfer, we calculated Bader charges for pristine FGT, an isolated TCNQ molecule, and the model FGT-TCNQ heterostructure (Table S2). These calculations revealed that the total charge on the Fe, Ge, and Te atoms increases from the charge-neutral state in pristine FGT to $+1.1$ in the FGT-TCNQ heterostructure, while the total negative charge on the TCNQ molecule increases from 0 to -1.1 when going from the neutral molecule to the heterostructure. Thus, the theoretical results confirm the charge transfer from FGT to TCNQ observed experimentally by IR and Raman spectroscopy, as discussed above.

Table 1: Adsorption energy (E_{ads}) for a single TCNQ molecule on a 5-atom-thick layer of FGT, with the center of TCNQ positioned above different atoms or bonds of the single FGT layer.

Location	E_{ads} (eV)	d_{min} (Å) ^[a]
Fe atoms	-3.09	2.619
Ge atoms	-3.14	2.557
Te atoms	-2.62	3.010
Fe–Te bonds	-2.90	2.691
Ge–Te bonds	-2.91	2.624
Fe–Ge bonds	-2.97	2.591

[a] The shortest distance between the TCNQ molecule and the FGT layer, along the layer normal.

Next, we calculated the magnetic anisotropy energy (MAE) in both the pristine FGT and upon TCNQ deposition, obtaining values of 1.086 meV and 0.984 meV per Fe atom for the former and the latter, respectively. This implies that the perpendicular anisotropy of the system slightly decreases upon TCNQ deposition, which arises from the effective transfer of electrons from FGT to TCNQ. This change in the MAE magnitude cannot justify the substantial increase in the coercivity of the FGT-TCNQ heterostructure.

On the other hand, it has been shown that the coercive field of FGT can be manipulated by gating, and the change in H_c was directly related to the strength of the interlayer exchange coupling (J_{int}) within the FGT structure.^[67] Consequently, we expect that the charge transfer from FGT to TCNQ can modulate the value of J_{int} in FGT. Figure 9 shows the computed variation in J_{int} (defined as the energy difference between the antiferromagnetic and ferromagnetic states) and the MAE for bulk FGT as a function of hole doping, which simulates the impact of TCNQ deposition at different concentrations. It can be seen that, while hole doping causes a reduction in MAE, the ferromagnetic nature of J_{int} increases more rapidly, justifying an enhancement in H_c . Hence, we attribute the dramatic increase in the coercivity of the FGT-TCNQ heterostructure to the effect of hole doping on the interlayer magnetic exchange in the FGT sheets.

Conclusions

This work demonstrates that liquid-phase exfoliation, with appropriate choice of organic solvent, provides a viable pathway for larger-scale production of nanosheets of the layered Fe_3GeTe_2 (FGT) ferromagnet. The nanosheets with the average thickness from 6 nm to 19 nm preserve the ferromagnetic behavior although the Curie temperature (T_c) gradually decreases with the decrease in the thickness

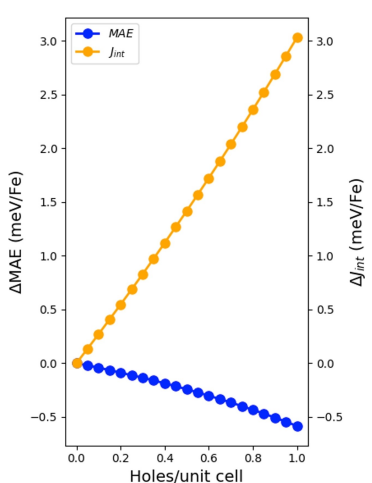


Figure 9. The effect of hole concentration on the values of magnetic anisotropy energy (MAE) and interlayer magnetic exchange coupling (J_{int}) in the bulk FGT.

and lateral dimensions of the nanosheets. Similar to the previously reported reactivity of the organic acceptor TCNQ toward metallic surfaces, such as Cu or Ag, we have observed the formation of FGT-TCNQ composites accompanied by electron transfer from the metallic nanosheets to organic molecules. Most remarkably, however, the composite material exhibits a 5-fold increase in coercivity as compared to the initially exfoliated FGT nanosheets. This increase was traced to the impact of hole doping on the interlayer magnetic exchange in the FGT structure. These findings suggest intriguing possibilities encoded in the chemistry of systems composed of 2D magnets and redox-active molecules. Our labs are currently exploring other types of such systems to understand how the combination of the magnetic and redox-active properties might dictate the magnetic behavior of related solid-molecule heterostructures.

Supporting Information

Detailed experimental and theoretical protocols used in this work, photographs of stepwise exfoliation and centrifugation procedure, additional PXRD patterns, Raman and IR spectra, SEM and TEM images, TGA data, magnetic plots, and theoretical results.

Acknowledgements

This work was supported by the National Science Foundation (awards DMR-1905499 and DMR-2233902). The Quantum Design MPMS-3 system used for magnetic measurements was acquired with support of the NSF MRI program (DMR-2216125). The TEM studies were performed at National High Magnetic Field Laboratory supported by the NSF Cooperative Agreement DMR-2128556 and the State of Florida. The project also used resources provided by the X-ray Crystallography Center (FSU075000XRAY) and the Materials Characterization Laboratory (FSU075000MAC) at the Department of Chemistry and Biochemistry, Florida State University. J.J.B. acknowledges the European Union (ERC-2021-StG-101042680 2D-SMARTIES) and the Generalitat Valenciana (grant CIDEXG/2023/1). A.M.R. thanks the Spanish MIU (Grant No FPU21/04195).

Conflict of Interest

The authors declare no conflict of interest.

Data Availability Statement

The data that support the findings of this study are available from the corresponding author upon reasonable request.

Keywords: 2D material · ferromagnet · heterostructure · liquid phase exfoliation · TCNQ

- [1] K. S. Novoselov, A. K. Geim, S. V. Morozov, D. Jiang, Y. Zhang, S. V. Dubonos, I. V. Grigorieva, A. A. Firsov, *Science* **2004**, *306*, 666–669.
- [2] A. K. Geim, K. S. Novoselov, *Nat. Mater.* **2007**, *6*, 183–191.
- [3] J. Liu, J. Tang, J. J. Gooding, *J. Mater. Chem.* **2012**, *22*, 12435–12452.
- [4] E. Coronado, *Nat. Rev. Mater.* **2020**, *5*, 87–104.
- [5] T. A. Shifa, F. Wang, Y. Liu, J. He, *Adv. Mater.* **2019**, *31*, 1804828.
- [6] X. Zhang, L. Zhang, J. D. Perkins, A. Zunger, *Phys. Rev. Lett.* **2015**, *115*, 176602.
- [7] K. F. Mak, J. Shan, D. C. Ralph, *Nat. Rev. Phys.* **2019**, *1*, 646–661.
- [8] Q. H. Wang, A. Bedoya-Pinto, M. Blei, A. H. Dismukes, A. Hamo, S. Jenkins, M. Koperski, Y. Liu, Q.-C. Sun, E. J. Telford, H. H. Kim, M. Augustin, U. Vool, J.-X. Yin, L. H. Li, A. Falin, C. R. Dean, F. Casanova, R. F. L. Evans, M. Chshiev, A. Mishchenko, C. Petrovic, R. He, L. Zhao, A. W. Tsen, B. D. Gerardot, M. Brotons-Gisbert, Z. Guguchia, X. Roy, S. Tongay, Z. Wang, M. Z. Hasan, J. Wrachtrup, A. Yacoby, A. Fert, S. Parkin, K. S. Novoselov, P. Dai, L. Balicas, E. J. G. Santos, *ACS Nano* **2022**, *16*, 6960–7079.
- [9] M. Ashton, J. Paul, S. B. Sinnott, R. G. Hennig, *Phys. Rev. Lett.* **2017**, *118*, 106101.
- [10] C. L. Tan, X. H. Cao, X. J. Wu, Q. Y. He, J. Yang, X. Zhang, J. Z. Chen, W. Zhao, S. K. Han, G. H. Nam, M. Sindoro, H. Zhang, *Chem. Rev.* **2017**, *117*, 6225–6331.
- [11] N. R. Glavin, R. Rao, V. Varshney, E. Bianco, A. Apte, A. Roy, E. Ringe, P. M. Ajayan, *Adv. Mater.* **2020**, *32*, 2070052.
- [12] Q. Ma, G. Ren, K. Xu, J. Z. Ou, *Adv. Opt. Mater.* **2021**, *9*, 2001313.
- [13] X. Liu, M. C. Hersam, *Nat. Rev. Mater.* **2019**, *4*, 669–684.
- [14] M. Chhowalla, D. Jena, H. Zhang, *Nat. Rev. Mater.* **2016**, *1*, 16052.
- [15] R. Kurapati, K. Kostarelos, M. Prato, A. Bianco, *Adv. Mater.* **2016**, *28*, 6052–6074.
- [16] L. Cheng, X. Wang, F. Gong, T. Liu, Z. Liu, *Adv. Mater.* **2020**, *32*, 1902333.
- [17] H. Liu, Y. Liu, D. Zhu, *J. Mater. Chem.* **2011**, *21*, 3335–3345.
- [18] V. Georgakilas, M. Otyepka, A. B. Bourlinos, V. Chandra, N. Kim, K. C. Kemp, P. Hobza, R. Zboril, K. S. Kim, *Chem. Rev.* **2012**, *112*, 6156–6214.
- [19] S. Bertolazzi, M. Gobbi, Y. Zhao, C. Backes, P. Samorì, *Chem. Soc. Rev.* **2018**, *47*, 6845–6888.
- [20] L. Daukiya, J. Seibel, S. De Feyter, *Advances in Physics: X* **2019**, *4*, 1625723.
- [21] A. R. Brill, E. Koren, G. de Ruiter, *J. Mater. Chem. C* **2021**, *9*, 11569–11587.
- [22] J. H. Jeong, S. Kang, N. Kim, R. Joshi, G.-H. Lee, *Phys. Chem. Chem. Phys.* **2022**, *24*, 10684–10711.
- [23] Z. Xie, B. Zhang, Y. Ge, Y. Zhu, G. Nie, Y. Song, C.-K. Lim, H. Zhang, P. N. Prasad, *Chem. Rev.* **2022**, *122*, 1127–1207.
- [24] H. Liu, M. Cui, C. Dang, W. Wen, X. Wang, L. Xie, *ACS Appl. Mater. Interfaces* **2019**, *11*, 34424–34429.
- [25] J. Wang, Z. Ji, G. Yang, X. Chuai, F. Liu, Z. Zhou, C. Lu, W. Wei, X. Shi, J. Niu, L. Wang, H. Wang, J. Chen, N. Lu, C. Jiang, L. Li, M. Liu, *Adv. Funct. Mater.* **2018**, *28*, 1806244.
- [26] X. Liu, J.-C. Ren, S. Zhang, M. Fuentes-Cabrera, S. Li, W. Liu, *J. Phys. Chem. Lett.* **2018**, *9*, 3897–3903.
- [27] C. Tang, L. Zhang, A. Du, *J. Mater. Chem. C* **2020**, *8*, 14948–14953.
- [28] D. L. Cortie, G. L. Causer, K. C. Rule, H. Fritzsche, W. Kreuzpaintner, F. Klose, *Adv. Funct. Mater.* **2020**, *30*, 1901414.

[29] B. Huang, G. Clark, E. Navarro-Moratalla, D. R. Klein, R. Cheng, K. L. Seyler, D. Zhong, E. Schmidgall, M. A. McGuire, D. H. Cobden, W. Yao, D. Xiao, P. Jarillo-Herrero, X. Xu, *Nature* **2017**, *546*, 270–273.

[30] S. A. López-Paz, Z. Guguchia, V. Y. Pomjakushin, C. Witteveen, A. Cervellino, H. Luetkens, N. Casati, A. F. Morpurgo, F. O. von Rohr, *Nat. Commun.* **2022**, *13*, 4745.

[31] C. Boix-Constant, S. Mañas-Valero, A. M. Ruiz, A. Rybakov, K. A. Konieczny, S. Pillet, J. J. Baldoví, E. Coronado, *Adv. Mater.* **2022**, *34*, 2204940.

[32] Y. Deng, Y. Yu, Y. Song, J. Zhang, N. Z. Wang, Z. Sun, Y. Yi, Y. Z. Wu, S. Wu, J. Zhu, J. Wang, X. H. Chen, Y. Zhang, *Nature* **2018**, *563*, 94–99.

[33] Z. Fei, B. Huang, P. Malinowski, W. Wang, T. Song, J. Sanchez, W. Yao, D. Xiao, X. Zhu, A. F. May, W. Wu, D. H. Cobden, J.-H. Chu, X. Xu, *Nat. Mater.* **2018**, *17*, 778–782.

[34] F. A. Ma'Mari, T. Moorsom, G. Teobaldi, W. Deacon, T. Prokscha, H. Luetkens, S. Lee, G. E. Sterbinsky, D. A. Arena, D. A. MacLaren, M. Flokstra, M. Ali, M. C. Wheeler, G. Burnell, B. J. Hickey, O. Cespedes, *Nature* **2015**, *524*, 69–73.

[35] G. A. Landrum, R. Dronskowski, *Angew. Chem. Int. Ed.* **1999**, *38*, 1390–1393.

[36] G. A. Landrum, R. Dronskowski, *Angew. Chem. Int. Ed.* **2000**, *39*, 1560–1585.

[37] G. D. Samolyuk, G. J. Miller, *J. Comput. Chem.* **2008**, *29*, 2177–2186.

[38] M. Shatruk, Ed. R. A. Scott *Encyclopedia of Inorganic and Bioinorganic Chemistry*, Wiley-VCH, Chichester **2017**, eibc2494.

[39] O. Gourdon, S. L. Bud'ko, D. Williams, G. J. Miller, *Inorg. Chem.* **2004**, *43*, 3210–3218.

[40] B. P. T. Fokwa, H. Lueken, R. Dronskowski, *Eur. J. Inorg. Chem.* **2011**, 3926–3930.

[41] P. Shankhari, P. R. N. Misra, M. Mbarki, H. Park, B. P. T. Fokwa, *Inorg. Chem.* **2017**, *56*, 446–451.

[42] K. Kovnir, W. M. Reiff, A. P. Menushenkov, A. A. Yaroslavtsev, R. V. Chernikov, M. Shatruk, *Chem. Mater.* **2011**, *23*, 3021–3024.

[43] X. Tan, G. Fabbri, D. Haskel, A. A. Yaroslavtsev, H. Cao, C. M. Thompson, K. Kovnir, A. P. Menushenkov, R. V. Chernikov, V. O. Garlea, M. Shatruk, *J. Am. Chem. Soc.* **2016**, *138*, 2724–2731.

[44] X. Tan, Z. P. Tener, M. Shatruk, *Acc. Chem. Res.* **2018**, *51*, 230–239.

[45] Y. Hernandez, V. Nicolosi, M. Lotya, F. M. Blighe, Z. Sun, S. De, I. T. McGovern, B. Holland, M. Byrne, Y. K. Gun'ko, J. J. Boland, P. Niraj, G. Duesberg, S. Krishnamurthy, R. Goodhue, J. Hutchison, V. Scardaci, A. C. Ferrari, J. N. Coleman, *Nat. Nanotechnol.* **2008**, *3*, 563–568.

[46] J. N. Coleman, *Acc. Chem. Res.* **2013**, *46*, 14–22.

[47] C. Backes, T. M. Higgins, A. Kelly, C. Boland, A. Harvey, D. Hanlon, J. N. Coleman, *Chem. Mater.* **2017**, *29*, 243–255.

[48] V. Y. Verchenko, A. A. Tsirlin, A. V. Sobolev, I. A. Presniakov, A. V. Shevelkov, *Inorg. Chem.* **2015**, *54*, 8598–8607.

[49] S. P. Ogilvie, M. J. Large, G. Fratta, M. Meloni, R. Canton-Vitoria, N. Tagmatarchis, F. Massuyeau, C. P. Ewels, A. A. K. King, A. B. Dalton, *Sci. Rep.* **2017**, *7*, 16706.

[50] P. Chavalekvirat, W. Hirunpinyopas, K. Deshorns, K. Jitapunkul, P. Iamprasertkun, *Precision Chem.* **2024**, *2*, 300–329.

[51] K. L. Ng, B. M. Maciejewska, L. Qin, C. Johnston, J. Barrio, M.-M. Titirici, I. Tzanakis, D. G. Eskin, K. Porfyrakis, J. Mi, N. Grobert, *ACS Sust. Chem. Eng.* **2023**, *11*, 58–66.

[52] D. S. Kim, J. Y. Kee, J.-E. Lee, Y. Liu, Y. Kim, N. Kim, C. Hwang, W. Kim, C. Petrovic, D. R. Lee, C. Jang, H. Ryu, J. W. Choi, *Current Applied Physics* **2021**, *30*, 40–45.

[53] R. A. Heintz, H. H. Zhao, O. Y. Xiang, G. Grandinetti, J. Cowen, K. R. Dunbar, *Inorg. Chem.* **1999**, *38*, 144–156.

[54] R. Otero, R. Miranda, J. M. Gallego, *ACS Omega* **2019**, *4*, 16906–16915.

[55] J. S. Chappell, A. N. Bloch, W. A. Bryden, M. Maxfield, T. O. Poehler, D. O. Cowan, *J. Am. Chem. Soc.* **1981**, *103*, 2442–2443.

[56] S. Matsuzaki, R. Kuwata, K. Toyoda, *Solid State Commun.* **1980**, *33*, 403–405.

[57] The Curie temperature (T_C) was determined by extrapolating the segments of the χ vs. T curves from the paramagnetic and ferromagnetic regimes and finding their intersection.

[58] Q. Li, M. Yang, C. Gong, R. V. Chopdekar, A. T. N'Diaye, J. Turner, G. Chen, A. Scholl, P. Shafer, E. Arenholz, A. K. Schmid, S. Wang, K. Liu, N. Gao, A. S. Admasu, S.-W. Cheong, C. Hwang, J. Li, F. Wang, X. Zhang, Z. Qiu, *Nano Lett.* **2018**, *18*, 5974–5980.

[59] A. F. May, S. Calder, C. Cantoni, H. Cao, M. A. McGuire, *Phys. Rev. B* **2016**, *93*, 014411.

[60] C. Tan, J. Lee, S.-G. Jung, T. Park, S. Albarakati, J. Partridge, M. R. Field, D. G. McCulloch, L. Wang, C. Lee, *Nat. Commun.* **2018**, *9*, 1554.

[61] S. Y. Park, D. S. Kim, Y. Liu, J. Hwang, Y. Kim, W. Kim, J.-Y. Kim, C. Petrovic, C. Hwang, S.-K. Mo, H.-j. Kim, B.-C. Min, H. C. Koo, J. Chang, C. Jang, J. W. Choi, H. Ryu, *Nano Lett.* **2020**, *20*, 95–100.

[62] H. L. Zhuang, P. R. C. Kent, R. G. Hennig, *Phys. Rev. B* **2016**, *93*, 134407.

[63] Y.-P. Wang, X.-Y. Chen, M.-Q. Long, *Appl. Phys. Lett.* **2020**, *116*, 092404.

[64] A. M. Ruiz, D. L. Esteras, D. López-Alcalá, J. J. Baldoví, *Nano Lett.* **2024**, *24*, 7886–7894.

[65] H.-J. Deiseroth, K. Aleksandrov, C. Reiner, L. Kienle, R. K. Kremer, *Eur. J. Inorg. Chem.* **2006**, *2006*, 1561–1567.

[66] D. Singh, S. K. Gupta, Y. Sonvane, S. Sahoo, *Nanotechnol.* **2017**, *28*, 495202.

[67] Q. Wu, Y. Zhang, Z. Cui, P. Liu, B. Xiang, Z. Li, Z. Fu, Y. Lu, *Adv. Funct. Mater.* **2023**, *33*, 2214007.

[68] G. Zheng, W.-Q. Xie, S. Albarakati, M. Algarni, C. Tan, Y. Wang, J. Peng, J. Partridge, L. Farrar, J. Yi, Y. Xiong, M. Tian, Y.-J. Zhao, L. Wang, *Phys. Rev. Lett.* **2020**, *125*, 047202.

Manuscript received: July 2, 2024

Accepted manuscript online: September 18, 2024

Version of record online: November 2, 2024